Optik 164 (2018) 527–537

Contents lists available at ScienceDirect

Optik

journal homepage: www.elsevier.de/ijleo

Original research article

Structural, optical and electrical characteristics of sulfur incorporated ZnSe thin films

E.R. Shaaban[a,*], A. Almohammedi[b], El Sayed Yousef[c,d], Gomaa A.M. Ali[e], Kwok Feng Chong[e], A. Adel[a], A. Ashour[b,f]

[a] Physics Department, Faculty of Science, Al–Azhar University, Assuit, 71542, Egypt
[b] Physics Department, Faculty of Science, Islamic University, P.O. Box 170, Al Madinah, Saudi Arabia
[c] Research Center for Advanced Materials Science (RCAMS), King Khalid University, Abha 61413, P.O. Box 9004, Saudi Arabia
[d] Physics Department, Faculty of Science, King Khalid University, P.O. Box 9004, Abha, Saudi Arabia
[e] Faculty of Industrial Sciences & Technology, Universiti Malaysia Pahang, Gambang, 26300 Kuantan, Malaysia
[f] Physics Department, Faculty of Science, Minia University, El Minia, Egypt

ARTICLE INFO

Article history:
Received 16 November 2017
Received in revised form 28 February 2018
Accepted 1 March 2018

Keywords:
ZnSeS
Thin films
Optical constants
Tunable energy Gap
Electrical conductivity

ABSTRACT

In the present study, polycrystalline materials of $ZnSe_{1-x}S_x$ (x = 0, 0.25, 0.5, 0.75 and 1) were prepared by a conventional solid-state reaction method. Thin films of $ZnSe_{1-x}S_x$ of about 1 μm have been produced using evaporation method. The importance of $ZnSe_{1-x}S_x$ compound is the tunability of band gap when incorporating S into the ZnSe. Adding S at the expense of Se in ZnSe to form Zn-Se-S, which has a wider energy gap window layer to permit more light to reach the junction of solar cell. Both of optical constants (n, k) and film thickness have been determined precisely in terms of envelop method. Optical absorption spectra showed that band gap values increase with increasing S content. The electrical conductivity of $ZnSe_{1-x}S_x$ was studied and exhibit two type of variation versus temperature. The activation energy of linear portion of the low temperature range is lower than the activation energy of linear portion of high temperature range and it increases with increasing the sulfur content in all films in both temperature ranges.

1. Introduction

Due to the fear of depletion of the knowing energy sources, the whole world has been turned to the attention of solar energy, since it is a clean and renewable. The buffer layer has a crucial effect on the efficiency of solar cell system. The buffer layer of CdS has a short band gap width of about 2.42 eV [1], so about of 20 %of the incident photons are absorbed. Subsequently it is not considered environmentally friendly and affect negatively on the efficiency of solar cell. Great efforts have been done to substitute CdS buffer layer by other nontoxic low absorbing materials. The most popular candidates were ZnS [2–4] and ZnSe [5–7]. ZnS and ZnSe belong to II—VI semiconducting binary systems and have effective applications in light emitting as well as laser diodes [8–10]. If ZnS and ZnSe combine, an effective heterostructures containing ZnS/ZnSe systems will produced. The presence of sulfur (S) in ZnSeS increases the band gap width, which increases the blue response of devices [11]. ZnSeS used as light emitting diodes, visible laser diodes, light emitters and a wavelength tunable UV photodetector [12].

* Corresponding author.
E-mail address: esam_ramadan2008@yahoo.com (E.R. Shaaban).

https://doi.org/10.1016/j.ijleo.2018.03.001
0030-4026/

In the present work, ZnSeS has been prepared using a mixture of the two compound ZnS and ZnSe by a ball milling. The most known method, evaporation technique, has been used to get thin films in order to study the structural, optical, and electrical properties. The X–ray diffraction has been used to investigate the microstructure of these films. Optical band gap, refractive index and other optical constants have been deduced using envelope method. Electrical conductivity of $ZnSe_{1-x}S_x$ films was measured in terms of four-probe method in the range of temperature extended from 300–440 K. The activation energy has been determined via the variation of conductivity against reciprocal of absolute temperature.

2. Experimental details

Polycrystalline materials of $ZnSe_{1-x}S_x$ (x = 0, 0.25, 0.5, 0.75 and 1) were prepared by a conventional solid-state reaction method. Using ball milling technique, Stoichiometric amounts of high–purity (99.999%) analytical grade ZnS and ZnSe powders purchased form Aldrich were mixed in a ball mortar for about 30 min according to the following reaction:

$$xZnS + (1 - x)ZnSe \rightarrow ZnSe_{1-x}S_x \quad (1)$$

The mixed powders were then pressed into a disk–shape pellet. Such pellets were used as the starting materials from which the thin film will be prepared, the same technique was proposed for different compound in our previous studies [13]. The compositions of $ZnSe_{1-x}S_x$ (x = 0, 0.25 0.5, 0.75 and 1) thin films were deposited by thermal evaporating the powdered samples from a resistance heating quartz glass crucible onto dried pre–cleaned glass substrate at a pressure of about 1×10^{-6} Pa, using a conventional coating unit (Denton Vacuum DV 502 A). During evaporation process, the thickness of the produced films was monitored using FTM6 thickness monitor. The thicknesses of the as–deposited films were studied at different compositions, in order to avoid the effect of film thickness. During the deposition process, the substrates were kept at temperature 400 K and the deposition rate was adjusted at 2 nm/s. Such a low deposition rate produces a film composition, which is very close to that of the bulk starting material [25]. The substrates were rotated at slow speed of 5 rpm, to obtain a homogenous and smooth film. X–ray powder diffraction (XRD) Philips diffractometry (1710), with Cu–K_α radiation (λ = 1.54056 Å) has been used to examine the phase purity and crystal structure of $ZnSe_{1-x}S_x$ (x = 0, 0.25 0.5, 0.75 and 1). 2θ ranged between 10° and 65° with step–size of 0.02° and step time of 0.6 s. The elemental composition of the films was analyzed by using energy dispersive X-ray spectrometer unit (EDXS) interfaced with a scanning electron microscope, SEM (JOEL XL) operating an accelerating voltage of 30 kV, which was used to study the morphology of the film. The relative error of determining the indicated elements does not exceed 2.3%. The transmittance (T) and reflectance (R) optical spectra of the deposited films were performed at room temperature using U–vis–NIR JASCO–670 double beam spectrophotometer. At normal incidence, the transmittance spectra were collected without substrate in the reference beam in the wavelength range 300–2500 nm, while the reflectance spectra was measured using reflection attachment close to normal incidence (∼5°). In these measurements, the effect of slit correction was eliminated by adjusting spectrophotometer-slit width at 8 nm, which is much less than the width of the interference peaks observed at transparency region of the samples under study. Electrical conductivity of $ZnSe_{1-x}S_x$ films was measured in terms of four-probe method in the range of temperature extended from 300–440 K. Indium coating was used as electrodes to make ohmic contacts to $ZnSe_{1-x}S_x$ layers.

3. Results and discussion

3.1. Structural properties

The XRD pattern for $ZnSe_{1-x}S_x$ (x = 0, 0.25, 0.5, 0.75 and 1) thin films onto glass substrate are shown on Fig. 1. The figure shows that the films have good crystallinity with the sphalerite (111) texture. There are significant shifts to higher angles of the (111) peaks for the films with incorporating S at expense of Se in $ZnSe_{1-x}S_x$ thin films. This shift may be attributed to the atomic radius of S atom (1.09 Å) is smaller than the atomic radius of Se atom (1.22 Å) and due to changes of the lattice parameter value [13,14]. The inset of Fig. 1 shows the shift of (111) peak when adding S at expense of Se for $ZnSe_{1-x}S_x$. Thus, the pure ZnSe has (111) the peak position at 27.18° (JCPDS # 01–071–5977), whereas for pure ZnS has (111) a peak position at 28.53° (JCPDS # 01–071–5975). The lattice structure does not change and remains a cubic ZnSe–like sphalerite structure while sulfur atoms occupy selenium sites within the lattice during film formation.

3.2. Optical properties

3.2.1. Calculations of refractive index and film thickness

Fig. 2 shows the transmittance and reflectance versus wavelength for

$ZnSe_{1-x}S_x$ (x = 0, 0.25, 0.5, 0.75 and 1) compositions. The transmittance and reflectance spectra of the $ZnSe_{1-x}S_x$ thin film exhibit peaks and valleys that are associated with interference effects. The optical measurements refer to that the compositions $ZnSe_{1-x}S_x$ (x = 0.25, 0.5, 0.75) have a transmittance and reflectance in between that of ZnS and ZnSe. Also Fig. 2 shows that addition of S at expense of Se can improve the transmission spectra, i.e. peaks and a valley goes toward higher transmission values. Fig. 3 shows the relation between the transmission and wavelength of the incident light for the five compositions under investigation.

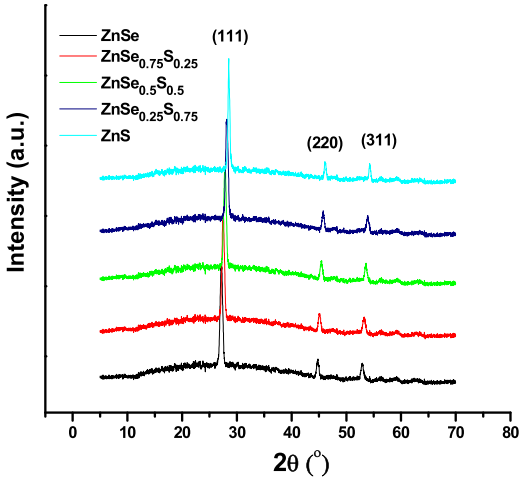

Fig. 1. X–ray diffraction patterns of polycrystalline $ZnSe_{1-x}S_x$ (x = 0, 0.25 0.5, 0.75 and 1) films prepared by thermal evaporation technique.

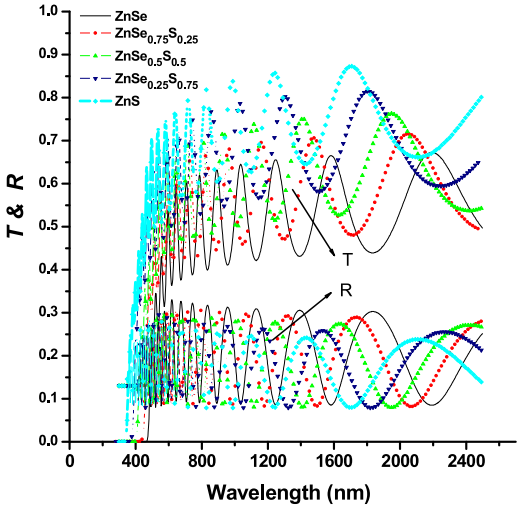

Fig. 2. A typical optical transmission–reflection spectra of polycrystalline $ZnSe_{1-x}S_x$ (x = 0, 0.25 0.5, 0.75 and 1) thin films.

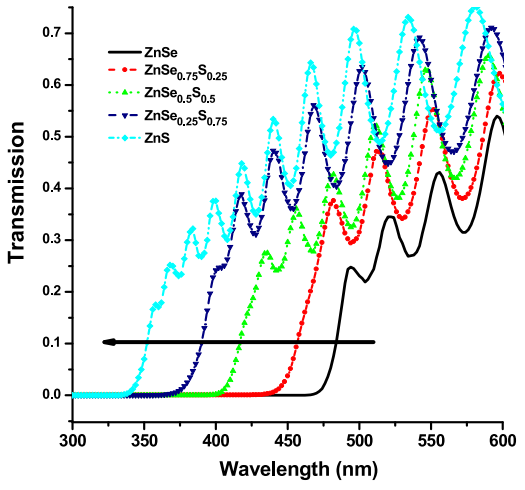

Fig. 3. Strong absorption region of optical transmission spectra of polycrystalline $ZnSe_{1-x}S_x$ (x = 0, 0.25 0.5, 0.75 and 1) thin films versus wavelength.

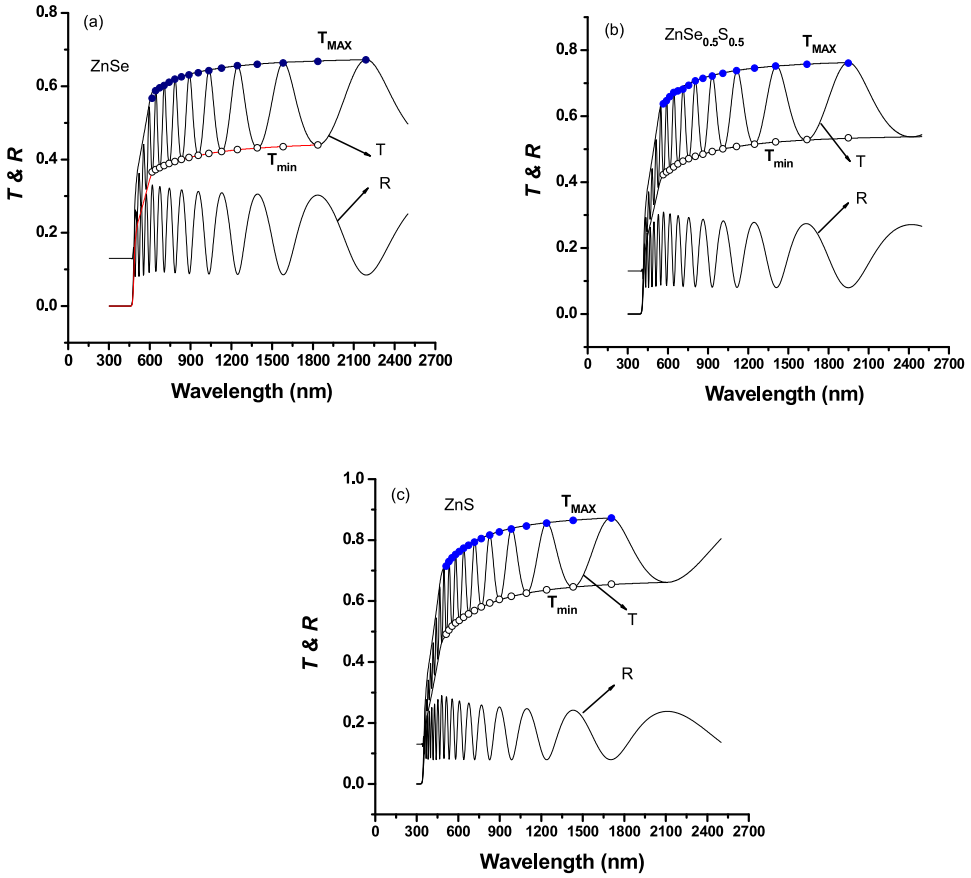

Fig. 4. A typical optical transmission–reflection spectra of (a) ZnSe, (b) $ZnSe_{0.5}S_{0.5}$ and (c) ZnS polycrystalline thin films. The top and bottom transmittance envelope T_{max} and T_{min} shown as filled circle and circle, respectively.

It was clear that the ZnS have the highest transmittance of about 0.65–0.75 according to the incident light of wavelength 465–580 nm and the lowest transmittance was for ZnSe (0.26–0.55) at the incident light of wavelength (495–595 nm). In addition, Fig. 3 shows a shift towards lower wavelengths in the strong absorption region of transmission spectra when increasing S in $ZnSe_{1-x}S_x$ thin film. Both thicknesses of the film, d and index of refraction, n of $ZnSe_{1-x}S_x$ thin films were estimated in terms of method of Swanepoal [15]. This method depends on the generating upper and lower envelopes through maximum and minimum transmissions (T_M, T_m) of the oscillating peak as shown in Fig. 4(a–c) for $ZnSe_{1-x}S_x$ (x = 0, 0.5, 1) thin films.

The main steps that have been considered in order to calculate both upper and lower envelope of transmission spectra are: i) data smoothing spline fit, ii) estimation of the location of the upper and lower tangential points of transmission spectra and iii) using the third–order of exponential decay in orgin7 (org. Lab. program) for interpolation through the estimated upper and lower tangential points. A distinct advantage of using the envelopes of the transmission spectrum rather than only the transmission spectrum is that, the envelopes are slow–changing functions of wavelength (λ), whereas the transmission spectrum varies rapidly with λ. Once the tangential points at λ_i, between the two envelopes and the transmission spectrum are known, the refractive index can be calculated.

In terms of Swanepoel's method the value of the refractive index of the film n_1, in the spectral region of medium and weak absorption, according to the expression [15,16].

$$n_1 = \left[N + \left(N^2 - s^2\right)^{1/2}\right]^{1/2} \tag{2}$$

where

$$N = 2s\frac{T_M - T_m}{T_M T_m} + \frac{s^2 + 1}{2}$$

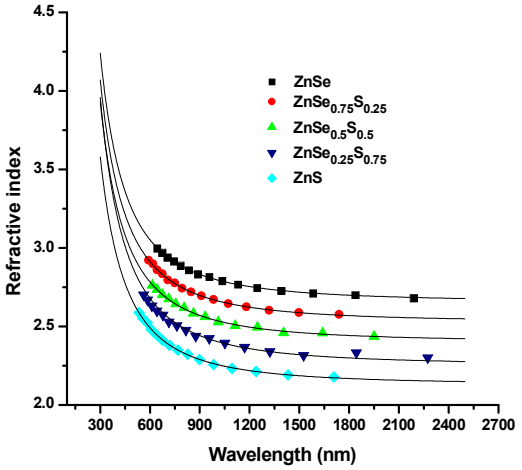

Fig. 5. Dispersion of refractive index of polycrystalline $ZnSe_{1-x}S_x$ (x = 0, 0.25 0.5, 0.75 and 1) thin films obtained from transmission spectra.

here T_M and T_m, are the transmission maximum and the corresponding minimum at a certain wavelength. On the other hand, the values of the refractive index of the substrate are obtained from the transmission spectrum of the substrate, T_s using the well–known equation as follows [17]:

$$s = \frac{1}{T_s} + \sqrt{\frac{1}{T_s} - 1} \tag{3}$$

Taking into account the basic equation for interference fringes:

$$2nd = m\lambda \tag{4}$$

where, m is the interference order and d is the film thickness. The interference order is integer for maxima and half–integer for minima. The d value can be calculated from the refractive index corresponding to adjacent extreme values (n_{el} and n_{e2}) at two maxima (or minima) at λ_1 and λ_2 through the following expression [18]:

$$d = \frac{\lambda_1\lambda_2}{2(\lambda_1 n_{e2} - \lambda_2 n_{e1})} \tag{5}$$

The values of d for the different samples were determined and listed as d_1 in Table 1. In order to increase the accuracy of d, integer or half integer values of m associated to each extreme and deriving a new thickness, d_2 from Eq. (4). The value of thickness of $ZnSe_{1-x}S_x$ (x = 0, 0.25 0.5, 0.75 and 1) thin films was about 1 μm as shown in Table 1. Again using the values of n_1 and the values of d that have a smaller dispersion ($\sigma 1 > \sigma 2$) for calculating the final accurate values of the refractive index n_2 in terms of Eq. (4) (Table 1). Now, the values of n can be fitted to a reasonable dispersion function such as the two-term Cauchy function, $n(\lambda) = B + A/\lambda^2$, which can be used for extrapolation the whole wavelength dependence of refractive index, see Fig. 5. In terms of he least squares fit of the three sets of values of n corresponding the three different composition samples, yields $n = 2.66 + 14.2 \times 10^4/\lambda^2$ for ZnSe, $n = 2.53 + 13.9 \times 10^4/\lambda^2$ for $ZnSe_{0.75}S_{0.25}$, $n = 2.40 + 13.8 \times 10^4/\lambda^2$ for $ZnSe_{0.5}S_{0.5}$, $n = 25 + 15.6 \times 10^4/\lambda^2$ for $ZnSe_{0.25}S_{0.75}$ and $n = 2.12 + 13.1 \times 10^4/\lambda^2$ for ZnS. Fig. 5 shows that the refractive index decreases with increasing wavelength of the incident light for all the compositions. It is clearly seen in Fig. 5 the change in the n values is related to the change in the composition, i.e. ZnSe has the higher values of refractive index, ZnS has the lowest values and $ZnSe_{0.5}S_{0.5}$ is intermediated between them. In Fig. 5, the values of n decrease with increasing S at expense of Se content because of the large atomic polarizability of Se atom (with atomic radius 1.22 Å) in comparison with the atomic polarizability of S (with atomic radius 1.09 Å) [19,20].

3.2.2. Determination of the extinction coefficient and optical band gap

Using the measured values of R and T in the strong absorption region, the absorption coefficient (α) can be calculated using the following equation [21]:

$$\alpha = \frac{1}{d} ln \left[\frac{(1-R)^2 + [(1-R)^4 + 4R^2T^2]^{\frac{1}{2}}}{2T} \right] \tag{6}$$

Fig. 6 displays the dependence of the absorption coefficient, α as a function of the photon energy ($h\nu$) for $ZnSe_{1-x}S_x$ (x = 0, 0.25, 0.5, 0.75 and 1) thin films at thickness of 1 μm.

It is shown that the spectral distribution of the absorption coefficient decreases with increasing the S content for $ZnSe_{1-x}S_x$ thin films.

Table 1
Values of λ, T_M and T_m for polycrystalline $ZnSe_{1-x}S_x$ (x = 0, 0.25 0.5, 0.75 and 1) corresponding to transmission spectra. The calculated values of refractive index and film thickness are based on the envelope method, obviously shown.

Samples	λ	T_M	T_m	s	n_1	d_1(nm)	m_0	m	d_2(nm)	n_2
ZnSe	644	0.5649	0.3719	1.532	2.9501	–	9.509	9.5	1036.9	2.995
	674	0.5725	0.3769	1.533	2.9388	1107.8	9.051	9	1032.1	2.97
	706	0.5781	0.3827	1.535	2.9155	1085.3	8.572	8.5	1029.2	2.938
	744	0.5869	0.3887	1.536	2.9013	1102.4	8.095	8	1025.8	2.914
	786	0.5952	0.3942	1.537	2.8893	1093.4	7.631	7.5	1020.1	2.886
	834	0.601	0.3996	1.539	2.8708	1055	7.145	7	1016.8	2.858
	890	0.6062	0.4051	1.54	2.8498	1020.8	6.647	6.5	1015	2.832
	958	0.6117	0.4108	1.54	2.8284	1018	6.129	6	1016.1	2.814
	1036	0.6173	0.4163	1.54	2.8085	1039.1	5.627	5.5	1014.4	2.79
	1130	0.6239	0.4216	1.539	2.7925	1035.1	5.13	5	1011.6	2.766
	1246	0.6303	0.4267	1.536	2.7759	1013.4	4.625	4.5	1009.9	2.745
	1392	0.6341	0.4314	1.532	2.7532	1004.7	4.106	4	1011.2	2.726
	1582	0.6376	0.4346	1.527	2.7372	999.05	3.592	3.5	1011.5	2.711
	1838	0.6416	0.439	1.521	2.7155	918.51	3.067	3	1015.3	2.699
	2190	0.6456	0.4614	1.523	2.597	–	2.462	2.5	1054.1	2.68
	$\bar{d}_1$ = *1038* nm σ_1 = *52.3* nm *(5 %)* $\bar{d}_2$ = *1021* nm σ_2 = *12.3* nm *(1.2 %)*									
$ZnSe_{0.75}S_{0.25}$	592	0.565	0.3811	1.526	2.8735	–	10.09	10	1030.1	2.921
	618	0.595	0.3949	1.527	2.8727	1100.3	9.658	9.5	1021.9	2.897
	644	0.6037	0.4047	1.529	2.8333	980.32	9.141	9	1022.8	2.86
	676	0.6102	0.4132	1.531	2.7975	1029.9	8.599	8.5	1027	2.835
	708	0.6151	0.4197	1.532	2.7711	1045.7	8.133	8	1022	2.795
	750	0.6208	0.4267	1.534	2.7451	1065.2	7.605	7.5	1024.6	2.776
	794	0.6297	0.4327	1.535	2.735	1120.8	7.157	7	1016.1	2.743
	848	0.6402	0.4394	1.536	2.7255	1072.2	6.678	6.5	1011.2	2.72
	910	0.6481	0.4458	1.537	2.7102	1047.6	6.188	6	1007.3	2.694
	984	0.6553	0.4522	1.537	2.693	1037.2	5.686	5.5	1004.8	2.671
	1072	0.6623	0.4584	1.537	2.6759	1023	5.187	5	1001.5	2.645
	1182	0.6687	0.4645	1.535	2.6571	1009.9	4.671	4.5	1000.9	2.625
	1318	0.6743	0.4701	1.532	2.6375	995.7	4.158	4	999.43	2.602
	1498	0.6787	0.4753	1.526	2.6152	977.9	3.627	3.5	1002.4	2.587
	1740	0.681	0.4794	1.52	2.5923	–	3.096	3	1006.8	2.576
	$\bar{d}_1$ = *1039* nm σ_1 = *43.4* nm *(4.2 %)* $\bar{d}_2$ = *1013* nm σ_2 = *10.7* nm *(1.1 %)*									
$ZnSe_{0.5}S_{0.5}$	614	0.6332	0.4361	1.53	2.7187	–	9.104	9	1016.3	2.761
	644	0.6452	0.4456	1.532	2.6973	1008.4	8.611	8.5	1014.7	2.735
	676	0.6501	0.4549	1.533	2.6581	981.33	8.084	8	1017.3	2.702
	714	0.6551	0.4631	1.535	2.6267	1066.6	7.564	7.5	1019.3	2.676
	756	0.6663	0.4705	1.537	2.6182	1159.2	7.121	7	1010.6	2.644
	806	0.6794	0.4774	1.538	2.6175	1123.9	6.677	6.5	1000.8	2.618
	862	0.6866	0.4841	1.539	2.6019	1036.8	6.206	6	993.9	2.584
	932	0.6933	0.4923	1.54	2.5772	1015.1	5.685	5.5	994.48	2.561
	1012	0.7008	0.5002	1.54	2.5562	1030.9	5.193	5	989.76	2.528
	1114	0.7087	0.5072	1.539	2.5402	990.32	4.688	4.5	986.74	2.505
	1248	0.7163	0.5142	1.536	2.5222	993.33	4.155	4	989.62	2.494
	1406	0.7223	0.5213	1.532	2.4983	969.97	3.653	3.5	984.87	2.459
	1640	0.7275	0.5287	1.525	2.469	960.15	3.095	3	996.35	2.458
	1950	0.7307	0.5335	1.52	2.4494	–	2.583	2.5	995.12	2.436
	$\bar{d}_1$ = *1028* nm σ_1 = *61.2* nm *(5.9 %)* $\bar{d}_2$ = *1001* nm σ_2 = *12.4* nm *(1.2 %)*									
ZnSe0.25S0.75	562	0.6596	0.4615	1.524	2.6368	–	9.571	9.5	1012.4	2.702
	586	0.6719	0.4703	1.525	2.623	1100	9.131	9	1005.3	2.669
	612	0.681	0.4806	1.527	2.5933	1042.3	8.643	8.5	1003	2.632
	642	0.6911	0.4912	1.529	2.5658	1016.9	8.152	8	1000.9	2.599
	678	0.7014	0.5019	1.531	2.5395	1075.7	7.64	7.5	1001.2	2.573
	714	0.7107	0.5106	1.532	2.5216	1094.9	7.204	7	991.02	2.529
	762	0.7209	0.5194	1.534	2.5062	1032.7	6.709	6.5	988.14	2.506
	816	0.7286	0.5278	1.536	2.4868	1040.5	6.216	6	984.39	2.477
	876	0.7357	0.5375	1.537	2.4602	985.77	5.729	5.5	979.19	2.438
	958	0.7458	0.5489	1.537	2.4336	977.41	5.182	5	984.12	2.424
	1052	0.7552	0.5578	1.537	2.4163	1015.6	4.685	4.5	979.58	2.395
	1170	0.7622	0.5659	1.535	2.3962	1004.3	4.178	4	976.55	2.368
	1322	0.7686	0.5728	1.532	2.3783	1003.6	3.67	3.5	972.73	2.341
	1526	0.7774	0.5794	1.526	2.365	943.09	3.161	3	967.85	2.316
	1844	0.7836	0.5872	1.518	2.3398	945.68	2.588	2.5	985.12	2.333
	2274	0.7846	0.5936	1.524	2.322	–	2.083	2	979.32	2.301

Table 1 (*Continued*)

Samples	λ	T_M	T_m	s	n_1	d_1(nm)	m_0	m	d_2(nm)	n_2
	$\bar{d}_1$ =1019 nm σ_1 = 49 nm (4.8 %) $\bar{d}_2$ = 988 nm σ_2 = 13.1 nm (1.3 %)									
ZnS	534	0.7011	0.5043	1.521	2.5173	–	9.703	9.5	1007.6	2.587
	556	0.7125	0.5171	1.523	2.4849	1042.4	9.199	9	1006.9	2.552
	582	0.7231	0.5274	1.525	2.4644	1135.5	8.716	8.5	1003.7	2.523
	608	0.7327	0.536	1.527	2.4496	1139.7	8.293	8	992.82	2.481
	640	0.7428	0.5463	1.529	2.4292	1067.5	7.813	7.5	987.98	2.448
	676	0.7525	0.557	1.531	2.4069	1048.8	7.329	7	983	2.413
	718	0.7624	0.5684	1.532	2.383	1024	6.831	6.5	979.24	2.38
	768	0.7733	0.5805	1.534	2.3595	1004.8	6.324	6	976.48	2.35
	828	0.7845	0.5929	1.536	2.336	1007.1	5.807	5.5	974.73	2.323
	898	0.7944	0.6046	1.537	2.313	1018.4	5.302	5	970.59	2.29
	984	0.8038	0.6153	1.537	2.293	1005.1	4.797	4.5	965.53	2.258
	1094	0.813	0.6256	1.537	2.2737	971.08	4.278	4	962.32	2.232
	1240	0.8221	0.6363	1.534	2.2511	958.81	3.737	3.5	963.96	2.213
	1432	0.8308	0.6461	1.529	2.2294	955.74	3.204	3	963.5	2.191
	1708	0.8386	0.6549	1.521	2.2072	–	2.66	2.5	967.29	2.178
	$\bar{d}_1$ =1029 nm σ_1 = 58.5 nm (5.7 %) $\bar{d}_2$ = 980 nm σ_2 = 16.1 nm (1.6 %)									

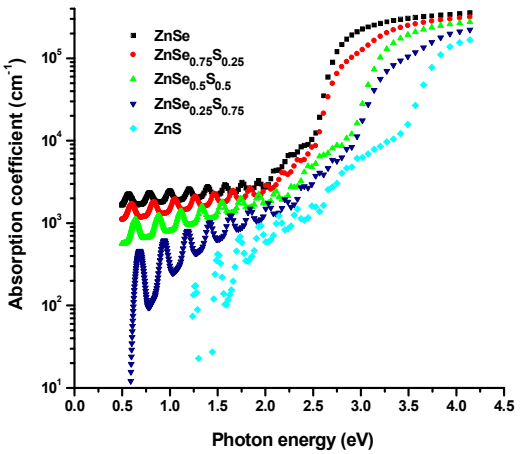

Fig. 6. The absorption coefficient, α versus photon energy $h\nu$ for the polycrystalline $ZnSe_{1-x}S_x$ (x = 0, 0.25 0.5, 0.75 and 1) thin films.

Extinction coefficient refers to several different measures of the absorption of light in a thin film. It can be calculated in terms of absorption coefficient, α using the following relation:

$$k = \frac{\alpha\lambda}{4\pi} \tag{7}$$

Fig. 7 shows the dependence of k as a function of wavelength. It is clear for all $ZnSe_{1-x}S_x$ thin films that k has higher value in the strong absorption region between both valance band and conduction band but at longer wavelength the value of k become nearly zero.

The energy gap values of $ZnSe_{1-x}S_x$ thin films were determined in terms of Tauc's relationship [22] in the strong absorption region ($\alpha \geq 10^4\ cm^{-1}$) as follows

$$\alpha(h\upsilon) = \frac{K(h\upsilon - E_g^{opt})^m}{h\upsilon} \tag{8}$$

where, K is a constant (independent of photon energy) [23], E_g^{opt} is the energy gap of investigated films that measured the energy between the top of valence and bottom of conduction band edges and m is a number, which characterizes the transition process. The value of m = 1/2 for allowed direct transition that occur in most crystalline semiconducting material has the value 2 for the indirect allowed transition for most amorphous semiconductors [22–26].

The energy band gap, E_g^{opt} can be determined by plotting the relation between $(\alpha h\nu)^m$ versus $h\nu$.

Figs. 8 illustrates $(\alpha h\nu)^2$ vs. $h\nu$ *for* $ZnSe_{1-x}S_x$ (x = 0, 0.25, 0.5, 0.75 and 1) thin films. This figure displays the best fitting between of $(\alpha h\nu)^2$ vs. $h\nu$, which confirms the allowed direct transition band gap for all compositions. The energy gap values were taken as the intercepts with the abscissa (at $(\alpha h\nu)^2 = 0$) as shown in Fig. 8. The direct energy gap values as a function of composition are shown in Fig. 9. The optical band gap E_g^{opt} increases from 2.68 to 3.67 eV with increasing S at expense of Se. The relationship between E_g^{opt} as a function of S content can be fitted in terms of parabolic equation as

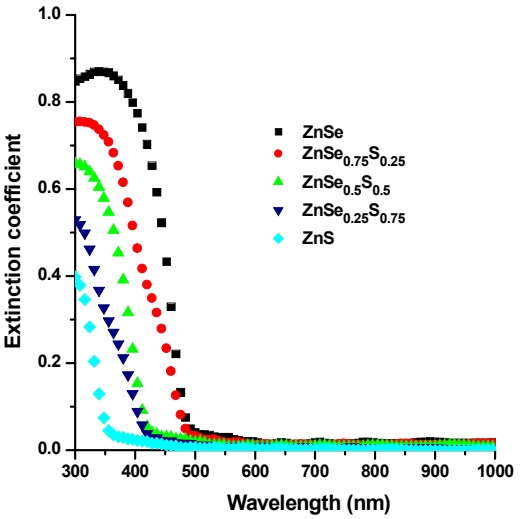

Fig. 7. The extinction coefficient, *k* versus wavelength, λ for polycrystalline $ZnSe_{1-x}S_x$ (x = 0, 0.25 0.5, 0.75 and 1)thin films.

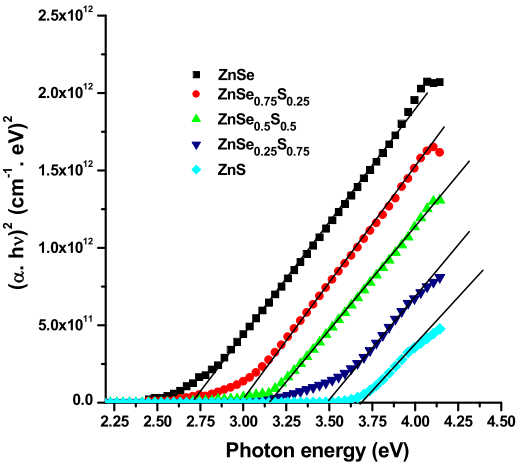

Fig. 8. The dependence of $(\alpha h\nu)^2$ on photon energy $h\nu$ for the different compositions of $ZnSe_{1-x}S_x$ (x = 0, 0.25 0.5, 0.75 and 1) thin films, from which the direct optical band gap E_g^{opt} is estimated.

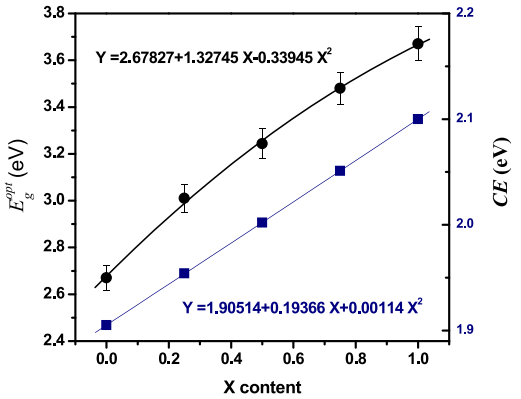

Fig. 9. Variation in optical energy gap, E_g^{opt} and cohesive energy, *CE* as a function. of S content.

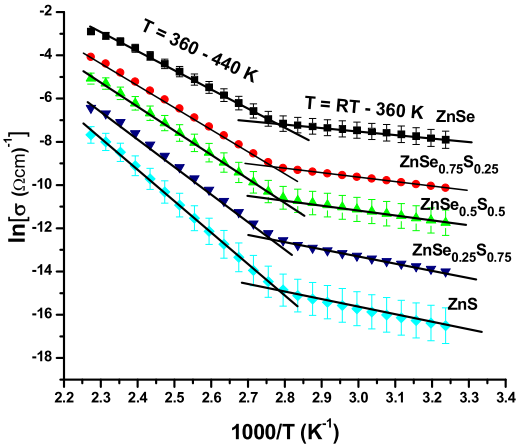

Fig. 10. Variation of electrical conductivity, $\boldsymbol{\sigma}$ versus of reciprocal of absolute. temperature for $ZnSe_{1-x}S_x$ (x = 0, 0.25 0.5, 0.75 and 1) thin films.

follows, Y = 2.67827 + 1.32745 X-0.33945 X^2. The two terminals of optical band gap are E_g^{opt} = 2.68 eV (for ZnSe) at x = 0 and E_g^{opt} = 3.67 eV (for ZnS) at x = 1. In the present work, the calculated values of E_g^{opt} for both ZnSe and ZnS are in a good agreement with that reported in previous work [27,28].

The increasing in optical band gap may be explained based on the increase in cohesive energy. The cohesive energy of these compositions was calculated according to relations and calculations given elsewhere [28–30]. Fig. 9 shows the variation in optical energy gap E_g^{opt} and cohesive energy, CE versus S content. This ensure the reason behind that the ZnSe has lowest energy gap but the energy gap widen as the incorporation of S to ZnSe to confirm the tenability of band gap of $ZnSe_{1-x}S_x$, which recommend these composition as a buffer layer of solar cell.

3.2.3. *Electrical conductivity of $ZnSe_{1-x}S_x$ thin films*

The D.C electrical conductivity of $ZnSe_{1-x}S_x$ (x = 0, 0.25, 0.5, 0.75 and 1) thin films varies with temperature according to Arrhenius relation [31–33]

$$\sigma = \sigma_0 e^{\frac{\Delta E}{KT}} \tag{9}$$

where σ_0 is a parameter depending on the semiconductor nature, K is the Boltzmann constant and ΔE is the thermal activation energy.

Fig. 10 shows the variation of D.C electrical conductivity against reciprocal of absolute temperature for $ZnSe_{1-x}S_x$ thin films with different temperatures at a range (300–440 K). This figure shows that the conductivity increases with increasing temperature over the all range of temperature. There are two portion stages of conductivity throughout the heating temperature range that exhibit two different straight lines as shown in Fig. 10. The first is the variation of low temperature region (300–360 K) and the conduction mechanism of this stage is due to carriers transport in/between localized (impurities) states near the valence and conduction bands and the second variation at high temperature region (360–440 K) and the conduction mechanism is due to the conduction of the carriers excited into the extended states beyond the mobility edge. These two conduction mechanism means that the D.C conductivity is non-linear with temperature. Fig. 10 shows the gradual decrease in conductivity at the increase of S content. The main reason of gradual decrease in conductivity is (i) increase of concentration of compensating complex defects, such as vacancy of zinc–shallow donor and (ii) The contact resistance of In- $ZnSe_{1-x}S_x$ at ZnS content ≥50% can reach several MΩ (contacts are not ohmic) [34]. Also, the decrease in conductivity with increasing S content of thin films might be explained by the presence of the crystallites with smaller size in respective samples. The obtained results might lead to the conclusion that the polycrystalline structure of the investigated samples plays an important role in the electronic transport properties. For polycrystalline samples it is possible to use the models elaborated for explaining the mechanism of electrical conduction in the films with discrete structure [35].

The activation energy of the two linear portions of $ZnSe_{1-x}S_x$ films are shown in Fig. 11. The values of the activation energies for both stages are declared to increase with increasing S content. On the other hand the activation energies of linear portion of the low temperature range are lower than the activation energy of linear portion of high temperature range. The obtained values of activation energy strongly differ from the values of band gap energy determined by optical measurements for $ZnSe_{1-x}S_x$ thin films. This suggests that the determined values of activation energy correspond to shallow donor or deep acceptor level located in the forbidden band of $ZnSe_{1-x}S_x$ [36].

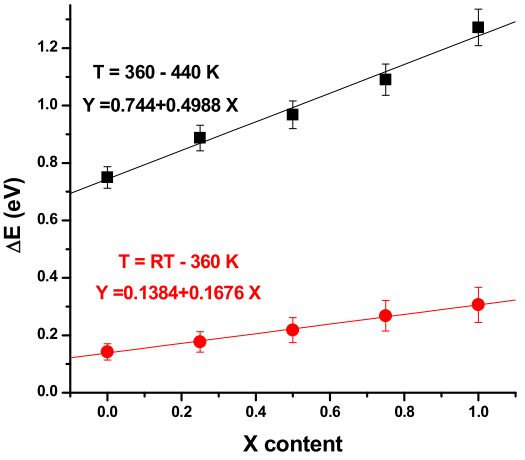

Fig. 11. Variation of activation energy of two portion region as a function of S. content.

4. Conclusions

Polycrystalline powder of $ZnSe_{1-x}S_x$ (x = 0, 0.25, 0.5, 0.75 and 1) have been prepared by ball milling technique by mixing of ZnSe and ZnS. The powder samples have been prepared as thin films by evaporation technique. X–ray diffraction has been used to emphasize the crystalline nature of these samples. There are significant shifts of the (111) peaks for the films with incorporating S at expense of Se in $ZnSe_{1-x}S_x$ thin films. This is attributed to that the atomic radius of S atom (1.09 Å) is smaller than the atomic radius of Se atom (1.22 Å). Swanepoel method has been introduced to find the film thickness, refractive index, and hence other optical parameters. It was found that the refractive index decreases with the incorporation of S to the ZnSe, over the entire spectral range, which is related to the increased polarizability of the larger Se atoms, in comparison with S atoms. A good fitting in the case of the optical direct gap was observed, according to Tauc relation, in the strong absorption region, further the non–direct gap was also determined. The results refer to that the energy gap increase with the addition of S to ZnSe in the two cases direct and indirect gaps, i.e. the energy gap widen as the incorporation of S to ZnSe to form $ZnSe_{0.5}S_{0.5}$ that recommend as a buffer layer of solar cell. This trend was discussed in terms of the cohesive energy of the compositions under investigation. The variation of conductivity against reciprocal of absolute temperature exhibit two different straight lines related to extrinsic and intrinsic conduction. The activation energy of linear portion of the low temperature range is lower than the activation energy of linear portion of high temperature range and it increases with increasing the sulfur content in all films in both temperature ranges.

Acknowledgment

The authors thank the Deanship of Scientific Research at King Khalid University (KKU) for funding this research project Number: (R.G.P.2/2/38).

References

[1] S. Armstrong, P.K. Datta, R.W. Miles, Thin Sol. Films 126 (2002) 403–404.
[2] J.Y. Park, R.B.V. Chalapathy, A.C. Lokhande, C.W. Hong, J.H. Kim, J. Alloys Compd. 695 (2017) 2652–2660.
[3] A.T. Salih, A.A. Najim, M.A.H. Muhi, K.R. Gbashi, Opt. Commun. 388 (2017) 84–89.
[4] M. Nguyen, K. Ernits, K.F. Tai, C.F. Ng, S.S. Pramana, W.A. Sasangka, S.K. Batabyal, T. Holopainen, D. Meissner, A. Neisser, L.H. Wong, Sol. Energy 111 (2015) 344–349.
[5] S.H. Lee, C. Jung, Y. Jun, S.-W. Kim, Opt. Mater. 49 (2015) 230–234.
[6] Z. Peng, Y. Liu, Y. Zhao, K. Chen, Y. Cheng, V. Kovalev, W. Chen, J. Alloys Compd. 587 (2014) 613–617.
[7] R. Kondrotas, M. Colina, M. Guc, M. Neuschitzer, S. Giraldo, X. Alcobé, F. Oliva, Y. Sánchez, P. Pistor, V. Izquierdo-Roca, A. Pérez–Rodriguez, E. Saucedo, Sol. Energy Mater. Sol. Cells 160 (2017) 26–33.
[8] Z. Liu, M. Osamura, T. Ootsuka, R. Kuroda, Y. Fukuzawa, N. Otogawa, Y. Nakayama, Y. Makita, H. Tanoue, J. Cryst. Growth 307 (1) (2007) 82–86.
[9] X.L. Zhu, L.W. Guo, N.S. Yu, J.F. Yan, M.Z. Peng, J. Zhang, H.Q. Jia, H. Chen, J.M. Zhou, J. Cryst. Growth 306 (2) (2007) 292–296.
[10] S. Armstrong, P.K. Datta, R.W. Miles, 22–26 October, Proceedings of the 17th European Photovoltaic Solar Energy Conference (2001) 1184.
[11] Y.P.V. Subbaiah, K.T.R. Reddy, Mater. Chem. Phys. 92 (2–3) (2005) 448–452.
[12] O.S. Kumar, S. Soundeswaran, R. Dhanasekaran, Mater. Chem. Phys. 87 (1) (2004) 75–80.
[13] R.G. Valeev, P.N. Krylov, E.A. Romanov, J. Surf. Invest. 1 (2007) 35–39.
[14] K.M.M. Abo-Hassan, M.R. Muhamad, S. Radhakrishna, Physica B 358 (2005) 256–264.
[15] R. Swanepoel, J. Phys. E: Sci. Instrum. 17 (1984) 896.
[16] E.R. Shaaban, I. Kansal, S.H. Mohamed, J.M.F. Ferreira, Physica B 404 (20) (2009) 3571–3576.
[17] T.S. Moss, Opt. Prop. Semicond. (London: Buttenvorths) (1959).
[18] R. Swanepoel, J. Phys. E: Sci. Instrum. 16 (1983) 1214–1222.
[19] S. Wemple, J. Gabbe, G. Boyd, J. Appl. Phys. 46 (1975) 3597–3605.
[20] E.R. Shaaban, M. El–Hagary, M. Emam–Ismail, M.B. El–Den, Philos. Mag. 91 (12) (2011) 1679–1692.

[21] R. Vahalova, L. Tichý, M. Vlcek, H. Ticha, Phys. Status Solidi A 181 (2000) 199–209.
[22] J. Tauc, Amorphous and Liquid Semiconductors, Plenum Press, New York, 1979, p. 159.
[23] E.A. Davis, N.F. Mott, Philos. Mag. 22 (1970) 0903–0922.
[24] M. Kastner, Phys. Rev. Lett. 28 (6) (1972) 355–357.
[25] N.F. Mott, Philos. Mag. 24 (1971) 935–958.
[26] E.R. Shaaban, I.S. Yahia, N. Afify, G.F. Salem, W. Dobrowolski, Mater. Sci. Semicond. Process 19 (2014) 107–113.
[27] E.R. Shaaban, J. Alloys Compd. 563 (2013) 274–279.
[28] E. Marquez, E.R. Shaaban, A.M. Abousehly, Int. J. New Hor. Phys. 1 (2014) 17.
[29] E.R. Shaaban, I.S. Yahia, E.G. El-Metwally, Acta Phys. Pol. A 121 (2012) 628.
[30] E.R. Shaaban, M.M. Soraya, M. Shapaan, H.S. Hassan, M.M. Samar, J. Alloys Compd. 693 (2017) 1052–1060.
[31] A.F. Qasrawi, N.M. Gasanly, Semicond. Sci. Technol. 20 (2005) 446–452.
[32] F. Yakuphanoglu, M. Sekerci, E. Evin, Physica B 382 (2006) 21–25.
[33] A.S. Maan, D.R. Goyal, S.K. Sharma, T.P. Sharma, J. Phys. III Fr. 4 (1994) 493–501.
[34] G.V. Colibaba, E.V. Monaico, E.P. Goncearenco, D.D. Nedeoglo, I.M. Tiginyanu, K. Nielsch, Semicond. Sci. Technol. 29 (2014) 125003.
[35] G. Hurbecke, Polycrystalline semiconductors, in: Physical Properties and Applications, Springer, Berlin, 1985.
[36] R.B. Kale, C.D. Lokhande, Appl. Surf. Sci. 252 (2005) 929–938.